JOURNAL OF APPLIED PHYSICS **114**, 174505 (2013)

A comprehensive picture of Cu doping in CdTe solar cells

J. Perrenoud, L. Kranz, C. Gretener, F. Pianezzi, S. Nishiwaki, S. Buecheler, and A. N. Tiwari

Laboratory for Thin Films and Photovoltaics, Empa—Swiss Federal Laboratories for Materials Science and Technology, Ueberlandstrasse 129, 8600 Duebendorf, Switzerland

(Received 23 August 2013; accepted 16 October 2013; published online 5 November 2013)

The importance of Cu for CdTe solar cell absorber doping has been increasingly recognized in recent years. Currently different models are being discussed how to understand the case of Cu_{Cd} substitutional doping in polycrystalline CdTe solar cells. In this work, an understanding is developed, which is based on a low concentration deep acceptor doped CdTe layer ($N_a \sim 5 \times 10^{14}\,cm^{-3}$, $E_a \sim 300\,meV$ above the valence band). Despite their non-shallow nature, Cu_{Cd} acceptors are fully or at least heavily (>30%) ionized. The low hole concentration in CdTe ($\sim 1 \times 10^{14}\,cm^{-3}$) originates directly from low Cu solubility in CdTe bulk material and is not caused by partial ionization or compensation as proposed by earlier models. The three to four orders of magnitude difference between bulk acceptor concentration and average Cu concentration in polycrystalline CdTe is attributed to grain boundary segregation of Cu. Our model is derived from substrate and superstrate CdTe solar cell measurements, controlled CdTe doping and quenching, Hall Effect measurements of CdTe films, numerical and analytical calculations, and a broad literature survey. Based on these results, routes to improve the conversion efficiency of CdTe solar cells are discussed. © *2013 AIP Publishing LLC*. [http://dx.doi.org/10.1063/1.4828484]

I. INTRODUCTION

Usually high efficiency CdTe thin film solar cells contain Cu, which has originally been introduced as back contact metal in 1969.[1] Since that time, the CdTe solar cell structure has been significantly modified, but Cu addition remained part of the back contact formation (see, for example, Ref. 2). Even though Cu was introduced at the back contact in all high efficiency solar cells, it has increasingly been realized that the importance of the fast diffusing Cu is beyond contact formation.

The importance of Cu for CdTe solar cells becomes evident whenever solar cells are processed without Cu or insufficient Cu amount using high purity source materials. In Figure 1, J-V curves of CdTe solar cells grown in substrate and superstrate configuration (see Figure 2) without Cu addition, insufficient Cu addition, and optimum Cu addition are shown. Solar cells without Cu addition (processed with high purity materials only) show an efficiency of <1%. The conversion efficiency increases from <1% to >13% upon Cu addition for substrate and superstrate devices (V_{oc} and J_{sc} improve see also Li *et al.*).[3]

In a recent work, Kranz *et al.*[4] have demonstrated that the specific Cu introduction position at the back contact is not crucial. Devices in substrate configuration without addition of Cu at the back contact, but with equal V_{oc} and fill factor (FF) compared to conventional superstrate devices were obtained. In these solar cells, Cu was introduced at the opposite side of the solar cells structure, before front contact deposition.[4]

It is well known that Cu can increase the p-type conductivity of CdTe[5] but the research community did so far not agree whether Cu is important for CdTe solar cell p-type doping or not. First principle calculation studies predict that Cu in CdTe occupies Cd sites,[6,7] where it acts as acceptor. This acceptor is non-shallow, situated ~300 meV above the valence band. Therefore, some authors question if such a deep acceptor might be able to increase the hole concentration in CdTe and attribute the role of Cu mainly to grain boundary passivation.[8] It is even possible that Cu atoms would lead to a resistivity increase, as they replace shallower Cd vacancy acceptors.[9] Other authors propose that Cu_{Cd} might be present with a concentration of $\sim 1 \times 10^{17}\,cm^{-3}$ and the widely observed hole concentration of $\sim 1 \times 10^{14}\,cm^{-3}$ might occur due to partial ionization and compensation.[10,11]

In this work, CdTe solar cells in substrate and superstrate configuration were investigated to access the problem of Cu doping. CdTe thin films directly deposited on glass (BSG Corning 7059) doped with Cu were additionally studied and numerical simulations were performed.

Based on the observations presented in this paper and further arguments, we propose that Cu_{Cd} is the dominant acceptor type defect in CdTe solar cells. The commonly observed hole concentration around $1 \times 10^{14}\,cm^{-3}$ in CdTe solar cells is not because of partial ionization or heavy compensation of a much higher deep acceptor concentration, but due to a low in-grain acceptor concentration which is heavily or fully ionized. The low acceptor concentration compared to the amount of introduced Cu atoms is explained by grain boundary segregation, based on thermodynamic equilibrium and non-equilibrium observations.

II. EXPERIMENTAL RESULTS AND DISCUSSION

A. Cu introduction and distribution in high efficiency CdTe solar cells

Figure 2 shows the schematics of superstrate and substrate CdTe solar cells and illustrates the position where Cu

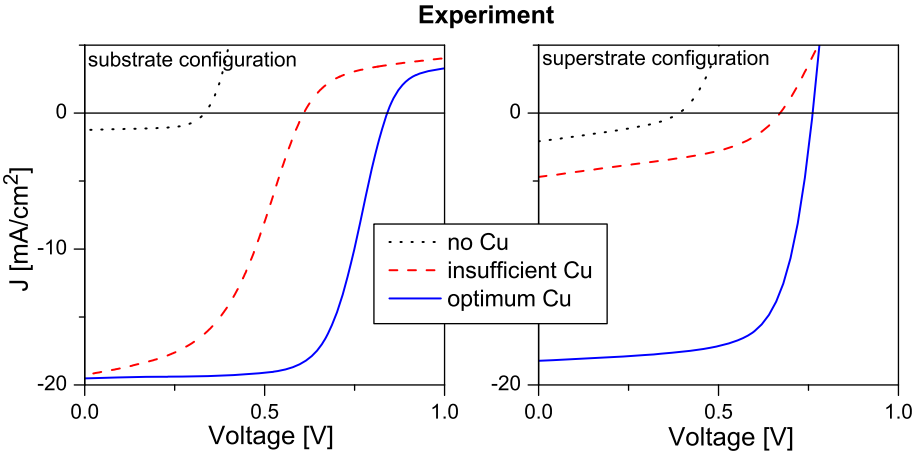

FIG. 1. J-V measurements of CdTe solar cells grown in substrate and superstrate configurations with different Cu amount added (0/0.1/1.0 Å (equivalent) in substrate and 0/2/32 Å in superstrate configuration). The J-V behavior can be modeled by the simulation shown in Figure 7.

is introduced to the device in this work. In superstrate configuration, Cu is added after $CdCl_2$ treatment often together with the back contact. Often the surface is chemically etched to create a Te rich surface region. Several nm Cu or Cu containing compounds are deposited and subsequently annealed at 150 °C–350 °C (e.g., ZnTe:Cu[3] C:HgTe:Cu_x[2] or Cu/Au).[12]

In substrate configuration, Cu was introduced from the opposite side. The Cu amount was 25 times lower (0.1 nm equivalent) with annealing temperature of 400 °C in oxygen containing ambient.

In Figure 2(b), the Cu distribution is compared for the two configurations as measured with time of flight secondary ion mass spectroscopy (TOF-SIMS). The devices exhibit a distinct Cu distribution, due to the difference in Cu amount added, the higher diffusion temperature in substrate configuration, and the surface etching performed in superstrate configuration. In both cases, Cu accumulation was detected at the front and back contact. Devices in substrate configuration show about one order of magnitude less Cu at the back contact compared to superstrate devices. The Cu amount detected inside CdS differs by a factor of 4. Inside the CdTe absorber layer, the Cu concentration is similar.

As both processes are well optimized and lead to nearly identical performance, this observation illustrates that Cu in CdTe is not a side effect but probably the most important aspect (see also Refs. 3, 5, 13, and 14). On the other hand, the device seems to be tolerant regarding Cu concentration in other layers.

B. Cu doping of CdTe films

In Figure 3, the impact of Cu doping on the dark conductivity of $CdCl_2$ treated CdTe layers on glass is shown. The resistivity drops by four orders of magnitude from 3×10^7 to 2×10^3 Ω cm upon addition of 8×10^{14} Cu atoms cm^{-2} (this corresponds to 1 Å Cu thickness equivalent, 0.01% Cu/CdTe atomic fraction, or an average of 2×10^{18} cm^{-3} Cu atoms per

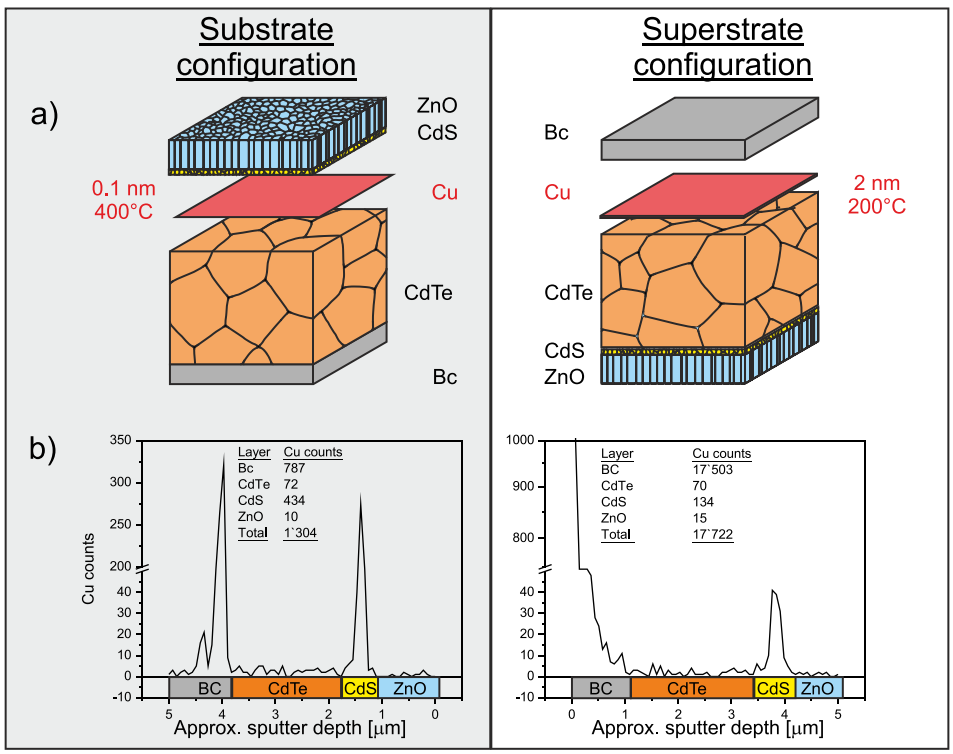

FIG. 2. Comparison of Cu introduction process (a) and Cu distribution (b) in optimum Cu doped substrate and superstrate solar cells. The different Cu introduction position leads to a difference in Cu concentration in front and back contact while the Cu concentration inside the CdTe absorber layer is similar.

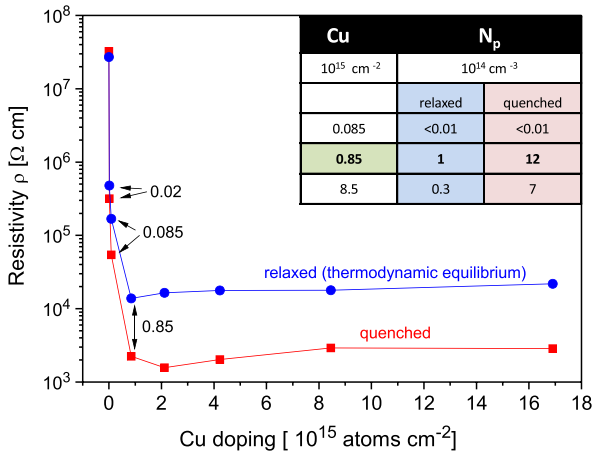

FIG. 3. Resistivity and Hall effect measurements of $CdCl_2$ treated CdTe thin films on glass doped with different amounts of Cu. Data in thermodynamic equilibrium are shown in blue (dots) and data in red (squares) are obtained after an annealing at 210 °C and subsequent quenching. The inset table shows the hole concentration (N_p) as measured with Hall Effect measurement.

volume). The layer reaches a maximum hole density of $\sim 1 \times 10^{14}\,\mathrm{cm}^{-3}$ in the relaxed state and $\sim 1 \times 10^{15}\mathrm{cm}^{-3}$ if quenched.

A resistivity drop by one order of magnitude is already observed after adding only 2×10^{13} Cu atoms cm^{-2} (2×10^{-6} atomic fraction Cu/CdTe). Note that Biglari *et al.*[5] reported a huge impact on CdTe resistivity upon introduction of an even smaller Cu amount in single crystals (see also Kucys *et al.*,[15] Chin *et al.*,[16] and Ma *et al.*[9]). This illustrates how sensitively this material reacts to Cu impurities. If not high purity source materials (at least 5N) are used the unintentional Cu concentration might already exceed ppm concentrations.

In Figure 3, it can be seen that above the optimum amount of Cu the resistivity increases again and the carrier concentration drops. The decrease in hole concentration can be attributed to the formation of compensating donors, e.g., Cu_i.[9]

C. Cu inactivity

As shown in Figure 2, the introduction of potentially $2 \times 10^{18}\,\mathrm{cm}^{-3}$ Cu atoms per CdTe volume leads to a 4 orders of magnitude lower hole concentration of $1 \times 10^{14}\,\mathrm{cm}^{-3}$. Also in solar cells, the measured Cu concentration in the CdTe layer ($5 \times 10^{17}\,\mathrm{cm}^{-3}$) (Refs. 3, 4, 14, and 17) is around 3 orders of magnitude higher than the apparent acceptor concentration.[13,14]

There are three main mechanisms which could explain this difference: compensation, partial ionization, and grain boundary segregation. Possible compensation mechanisms have been discussed by Kucys *et al.*[15] For example, the compensation by Cd_i by the reaction $Cu + Cd_{Cd} \rightarrow Cu_{Cd}^{-} + Cd_i^{+}$ or the compensation by Cu interstitial $Cu_{Cd}^{-} + Cu \rightarrow Cu_{Cd}^{-} + Cu_i^{+}$. The possibility of partial ionization in combination with compensation has been discussed in the work of Chin.[11] The third option, grain boundary segregation, will be discussed in Sec. II D.

D. Cu solubility limitation and grain boundary segregation

According to first principle calculations, it can be expected that Cu atoms at CdTe grain boundaries (GB) are energetically favored[8] compared to sites inside the CdTe bulk. Hence it is a reasonable assumption that Cu preferentially occupies these GB sites. In a higher Cu concentration regime, this has already been observed in the TEM study of Yan *et al.*[18]

An additional indicator how Cu is distributed inside polycrystalline CdTe is the bulk solubility of Cu in CdTe. The solubility of Cu in CdTe single crystals has been measured by Woodbury *et al.*,[19] Grytsiv *et al.*,[20] and Jones *et al.*[21] in the temperature range of 400–1000 K. As shown in Figure 4(b), an extrapolation of their data suggests Cu solubility between 3×10^{13} and 3×10^{14} Cu atoms cm^{-3} in single crystals at room temperature.

The solubility is not an absolute limitation for Cu concentration at a respective temperature. The concentration can exceed the room temperature solubility by fast cooling the CdTe from a higher temperature. If the diffusion constant of a dopant is low enough, a dopant concentration above solubility limit can persist for hours, days, or even years as it was, for example, demonstrated for the Li_{Cd} acceptor in CdTe by Desnica and Urli.[22] The possibility of such a metastable defect concentration in excess of solubility has also been shown using a numerical Cu migration model by Teeter and Asher.[17]

Recent calculations by Krasikov *et al.*[7] and the experimental work of Jones *et al.*[21] have shown that the diffusion constant of Cu_{Cd} acceptors is around 1×10^{-10} cm^2 s^{-1} at

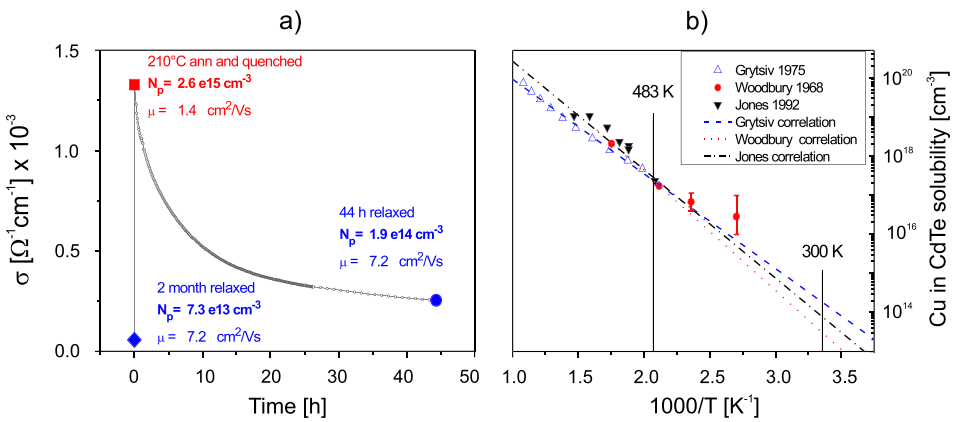

FIG. 4. Rise and decay of Cu doped CdTe thin film in plane conductivity upon additional 210 °C annealing with subsequent quenching by dipping into ice water (a). Cu in CdTe single crystall solubility after Refs. 19–21. (b). Extrapolation of the relation suggests that the room temperature Cu solubility is around 1×10^{14} Cu atoms cm^{-3}.

200 °C. Hence at 200 °C, Cu_{Cd} can diffuse μm distances within minutes inside the CdTe bulk. At room temperature, Cu_{Cd} diffusion over μm distances is slower and takes hours.[7] We can therefore expect that supersaturated polycrystalline CdTe:Cu can be generated by annealing at 200 °C for a few minutes and subsequent quenching. The supersaturation would decay within hours at room temperature as the distance for Cu atoms to reach grain boundary positions is in the order of a μm.

In Figures 3 and 4(a), the change in conductivity of a polycrystalline CdTe:Cu film upon heating to 210 °C and subsequent quenching is shown. Also shown in Figures 3 and 4 is that the higher conductivity originates from an increased hole concentration.

This observation can be well explained by the above described mechanism of supersaturation. It can be assumed that Cu from grain boundary positions diffused into the CdTe bulk material and lead to a higher bulk acceptor concentration. The subsequent decay of the hole concentration shown in Figure 4(a) can be attributed to Cu out diffusion. It is also assumed that concentration of cadmium vacancies is thereby not increased, as V_{Cd} also accumulate at grain boundaries.[23] According to the calculation of Du,[24] the diffusion barrier for Cd vacancies (V_{Cd}) and Cu_{Cd} is similar, 1.08 eV and 1.03 eV, respectively.

In Cd rich CdTe and or if the Fermi energy is close enough to the valence band, Cu is expected to additionally occupy interstitial sites (Cu_i) and act as a donor.[6,7] Krasikov *et al.*[7] have calculated that the Cu_i donor is a much faster diffusor than the Cu_{Cd} acceptor. If two dopant species with different diffusion speed are present in a material, one would expect to observe a two phase behavior. In analogy to the case of Lithium, a decompensation effect upon quenching should occur, given that Cu_i are also present in the material.[22] The Cu_i impurities should leave the CdTe bulk material faster than the Cu_{Cd} acceptor leading to an initial conductivity increase due to reduced compensation.

Such a conductivity increase could not be observed in any of our experiment. The absence of such an initial conductivity increase indicates that Cu_i donors have not formed in a relevant concentration inside the grains (compare with Ref. 22). The assumption that Cu_i did not form is in agreement with the calculation of Wei and Zhang if one assumes that the CdTe is Te rich.[6] The incorporation of oxygen could lead to such Te rich conditions by isovalent substitution of Te. Oxygen is present during $CdCl_2$ treatment and Cu diffusion annealing and it has been shown that oxygen can be incorporated in CdTe crystals with $\sim 1 \times 10^{16}\,cm^{-3}$ concentrations at least.[25] Also the fact that the hole concentration can be increased by quenching indicates that the in-grain acceptor concentration is solubility limited.

The above considerations of low solubility and fast diffusion of Cu suggest that inside the polycrystalline CdTe, most Cu atoms are situated at GB positions at room temperature in thermodynamic equilibrium. In the undoped CdTe film, the unintentional overall Cu concentration can reach $\sim 10^{14}\,cm^{-3}$ due to residual impurities (see material purity in the Experimental section). However, a hole concentration $< 10^{12}\,cm^{-3}$ and a resistivity above $10^7\ \Omega$ cm were measured for such undoped films. This could be explained by the assumption that also in this concentration regime Cu segregates to grain boundaries and does hardly dope the CdTe bulk.

In the doped CdTe film, the total Cu in polycrystalline CdTe film concentration is $\sim 10^{18}\,cm^{-3}$ including grain boundaries while the Cu_{Cd} in-grain concentration is probably in the 3×10^{13}–$3 \times 10^{14}\,cm^{-3}$ range reaching bulk saturation. Upon annealing and quenching, the in-grain Cu_{Cd} concentration can be increased temporarily at the expense of Cu at grain boundaries.

E. Cu_{Cd} acceptor: Position in the bandgap and degeneracy

From first principle calculations, it is expected that Cu induces a deep acceptor when occupying Cd sites (Cu_{Cd}). The position of the Cu_{Cd} acceptor above the valence band was calculated to be 220 meV by Wei and Zhang[6] and 310 meV by Krasikov *et al.*[7] Many experimental studies suggest an even deeper position around 350 meV above the valence band[5,26–29] while some experiments and earlier calculations suggest a position around 150 meV above the CdTe valence band.[30,31] In this work, it is assumed that the Cu_{Cd} acceptor is situated between 220 meV to 350 meV above the valence band following the more recent publications.[5–7]

Acceptors in CdTe are fourfold degenerate and each acceptor can be occupied by four electrons.[32] However, the ionization energy for multiple occupations will increase if the acceptor is already occupied due to coulomb interaction. There is not sufficient data available to model the situation in detail. Therefore, in the following, the Cu_{Cd} acceptor is treated as single acceptor. Nevertheless, one should keep in mind that the apparent acceptor concentration could be up to four times higher than the physical Cu solubility. The activation energy could be interpreted as medium activation energy of multiple Cu_{Cd} charging states. Due to the acceptor degeneracy, the apparent acceptor concentration in CdTe is in the following assumed to be in the range of $3 \times 10^{13}\,cm^{-3}$ to $1.2 \times 10^{15}\,cm^{-3}$.

F. Partial ionization

It might be puzzling that an acceptor ~10*kT above the valence band can be a relevant or even efficient p-dopant at room temperature. Using a thermal activation law,

$$\frac{N_a^-}{N_a} \propto \exp\left(\frac{-E_a}{2kT}\right) \tag{1}$$

would lead to a low ionization degree (1×10^{-4}) for an acceptor 300 meV above the valence band. However, the simplified expression (1) is only valid for shallow acceptors ($E_a < 50$ meV) and/or high concentrations ($1 \times 10^{18}\,cm^{-3}$) at room temperature. These conditions are not fulfilled in the case of CdTe:Cu discussed here.

For deep dopants ($E_a \gg kT$) at low concentration (non degenerate conditions) and not too low temperatures, an analytical expression to describe dopant occupation can be derived (see Ref. 32, page 122, Eq. (321.5), and the application example[33]). Here, the equation is given for a single acceptor.

$$\xi_a = \frac{N_a^-}{N_a} = \frac{-1 + \sqrt{1 + 4\ \frac{N_a}{N_V}\ \exp\left(\frac{E_a}{k_B T}\right)}}{2\ \frac{N_a}{N_V}\exp\left(\frac{E_a}{k_B T}\right)}, \quad (2)$$

where ξ_a is the acceptor ionization degree, N_a is the acceptor concentration [cm^{-3}], N_a^- is the ionized acceptor concentration [cm^{-3}], N_V is the effective density of states in the valence band [cm^{-3}], E_a is the acceptor activation energy (position above valence band) [eV], k_B is the Bolzmann constant [eV], and T is the temperature [K].

For the case of low enough acceptor concentration $N_a/N_V < \frac{1}{4}\ \exp(\frac{-E_a}{k_B T})$, the square root in the numerator can be expanded as Taylor series $\sqrt{1+x} = 1 + \frac{1}{2}x - \frac{1}{8}x^2 \ldots$, and higher order terms can be neglected. Formula 2 then simplifies to

$$\xi_a = 1 - \frac{N_a}{N_V}\ \exp\left(\frac{E_a}{k_B T}\right). \quad (3)$$

The ionization degree ξ_a always approaches 1 as the acceptor concentration N_a decreases. Therefore, also deep acceptors are fully ionized as long as their concentration is low enough. If we assume, for example, $E_a = 300\,\text{meV}$, $N_a = 1 \times 10^{13}\,\text{cm}^{-3}$, $N_V = 1.8 \times 10^{19}\,\text{cm}^{-3}$, and $T = 300\,\text{K}$, we get an ionization degree ξ_A of 95% and 94% using formula (2) or the simplified approximation formula (3), respectively.

In Figure 5, the ionization degree of acceptors depending on their depth and concentration is shown as calculated solving the basic semiconductor equations numerically using the program SCAPS[34] (see Experimental section). This calculation additionally includes the presence of $2 \times 10^{14}\,\text{cm}^{-3}$ donor type midgap defects (MGDFs), which are needed to realistically simulate CdTe solar cells. This MGDF cannot be considered using formula 2, therefore, SCAPS was used. However, the difference between the SCAPS calculation and formula 2 is small and formula 2 does still provide a good estimate of acceptor ionization degree in the CdTe solar cells. As we assume, for example, $E_a = 300\,\text{meV}$, $N_a = 5 \times 10^{14}\,\text{cm}^{-3}$, $N_V = 1.8 \times 10^{19}\,\text{cm}^{-3}$, and $T = 300\,\text{K}$, an ionization degree of 44% and 43% is predicted by SCAPS with MGDF and formula 2, respectively.

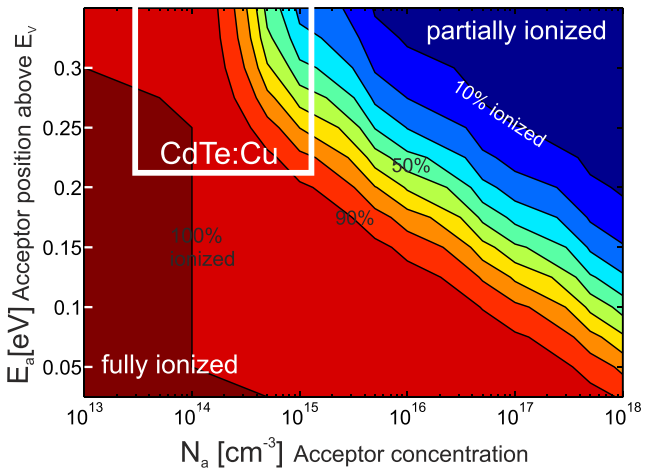

FIG. 5. Ionization degree ($\xi_a = N_a^-/N_a$) of acceptors in CdTe calculated with SCAPS. The white box indicates the region where CdTe:Cu bulk doping is suspected.

The apparent acceptor concentration in high efficiency CdTe solar cell absorbers is suspected to be in the range between $3 \times 10^{13}\,\text{cm}^{-3}$ and $1.2 \times 10^{15}\,\text{cm}^{-3}$ (solubility multiplied with acceptor degeneracy) as explained in the previous sections. This doping regime, where Cu_{Cd} bulk doping is suspected (3×10^{13}-$1.2 \times 10^{15}\,\text{cm}^{-3}$), is marked with a white square in Figure 5. In this regime, an ionization degree in the range of 30% to 100% can be expected despite the deep position of the acceptor in the bandgap. In other words: Partial ionization leads to less than one order of magnitude difference between hole concentration and acceptor concentration.

G. The space charge region (SCR) argument

In Sec. II F, the situation in the CdTe bulk far away from the surface/junction was analyzed. In the CdTe device, however, a p-n junction is present, which generates a SCR. Electrons from the CdS diffuse into CdTe and lift up the electron Fermi energy. Hence, inside the SCR, the Cu_{Cd} acceptor level is pushed below the Fermi energy in any case.

Therefore, the width of the SCR can be used to estimate the net acceptor concentration despite the problem that the position of the Cu_{Cd} acceptor in the bandgap is still only vaguely known (220–350 meV).

For example, in a substrate configuration CdTe solar cell, which was doped with 8×10^{14} Cu atoms cm^{-2}, a SCR size of 2.2 μm is measured with CV measurements. In order to adjust the SCAPS model of the device to get the same SCR width, a single acceptor concentration of $4 \times 10^{14}\,\text{cm}^{-3}$ is needed (including $2 \times 10^{14}\,\text{cm}^{-3}$ compensating MGDF donors) independent of the energetic position of the acceptor. Note the detail that in the SCR, the Fermi energy is sufficiently high above the valence band to enable multiple charging of the Cu_{Cd} acceptor and therefore the physical Cu_{Cd} acceptor density may be up to a factor four below the single acceptor concentration in the model.

The fact that the SCR provides an acceptor depth independent ionization mechanism supports the theory of low net acceptor concentration in CdTe.

A low hole concentration alone can also be explained by other models, as for example proposed by Chin.[11] In the example shown in his work, $N_A = 1 \times 10^{17}\,\text{cm}^{-3}$ and $N_D = 1 \times 10^{16}\,\text{cm}^{-3}$, the low hole density can successfully be explain but the resulting SCR width would be 200 nm only which is in disagreement with experimental observations.

Unless additional assumptions are introduced, the commonly observed SCR size of more than one μm is not compatible with a high acceptor concentration understanding of the CdTe solar cell.

III. NUMERICAL MODELING

A. Shockley-Read-Hall (SRH) recombination and model calibration

In CdTe thin film solar cells, deep defect assisted SRH recombination is believed to be the dominant recombination

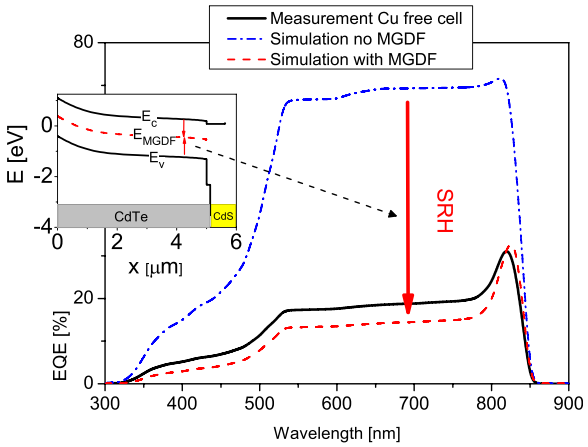

FIG. 6. An undoped (no Cu addition) CdTe solar cell exhibits strong recombination already under short circuit conditions leading to a reduced EQE (black solid line). This can be modeled using SCAPS by assuming an acceptor free devices (red dashed line). The calculated band diagram (inset graph) shows little band bending close to the CdTe/CdS interface, therfore, as carriers are not separated, the strong recombination occures via MGDF. The blue dashed-dotted line shows the calculated EQE without MGDF.

mechanism. A short discussion is provided here as SRH recombination is an important part of the following simulations.

According to first principle calculations, the intrinsic donor defects V_{Te} is close to midgap and hence an efficient recombination center.[6] Also a O_{Te}-H complex[34] or other deep defects might be relevant recombination centers. In the numerical model discussed in this paper, all these defects are represented by one mid-gap defect (MGDF).

Under short circuit conditions, SRH recombination is close to zero in standard CdTe solar cells, as the strong electric field in the SCR separates the carriers fast enough. The quantum efficiency (QE) measurement reveals only little recombination in short circuit conditions (see, for example, Ref. 36). In a Cu free, undoped device, the situation is essentially different. The inset of Figure 6 shows the energy band diagram of such a device, illuminated and in short circuit as calculated with SCAPS. The bands are flat close to the CdTe/CdS interface in agreement to electron beam induced current (EBIC) measurements performed by Kranz *et al.*[4] Due to the absence of a dominating separating field, such a Cu free device can visualize SRH recombination and allows calibration of the numerical model.

In Figure 6, the quantum efficiency of a Cu free substrate configuration solar cell is shown and compared to SCAPS simulations of an acceptor free device. The red dashed line in Figure 6 has been calculated using the values of $2 \times 10^{14}\,\mathrm{cm}^{-3}$ for MGDF concentration and $1 \times 10^{-13}\,\mathrm{cm}^{-2}$ for the hole capture cross section as proposed by Scheer and Schock.[37] These values can well reproduce the measurements. As no MGDF is assumed, the EQE is greatly overestimated (blue dashed-dotted line). Note also the collection peak at long wavelength which originates from carrier separation by the back contact field, which is effective for deep penetrating photons only.

We can summarize that comparison of Cu free devices with SCAPS simulations allows calibrating the MGDF concentration and thereby adjusting the recombination rate of model and measurement.

B. Modeling the impact of Cu on the solar cell J-V behavior

The dual experimental approach (substrate/superstrate configurations) can well illustrate the bivalent role of Cu in CdTe solar cells: Back contact barrier reduction and bulk doping.

Figure 1 shows two sets of measured J-V curves of CdTe solar cells in substrate and superstrate configurations with varying Cu amount added. As illustrated in Figure 2, in superstrate configuration solar cells, Cu was introduced from the back contact side; while in substrate configuration, Cu was introduced from the front contact side. It is also visible that in superstrate configuration, a larger amount of Cu is present at the back contact interface. With the knowledge on Cu doping and distribution, the six J-V curves shown in Figure 1 can now be interpreted.

It is assumed that Cu in CdTe leads to an increased acceptor concentration N_a; and additionally at the back contact interface, it reduces the majority carrier barrier height φ.[38] The simulated J-V curves are shown in Figure 7.

Solar cells with $N_a = 0$ in Figure 7 correspond to "no Cu" solar cells in Figure 1. The Cu respectively acceptor free solar cells exhibit a low J_{sc} and V_{oc}. The reduced built

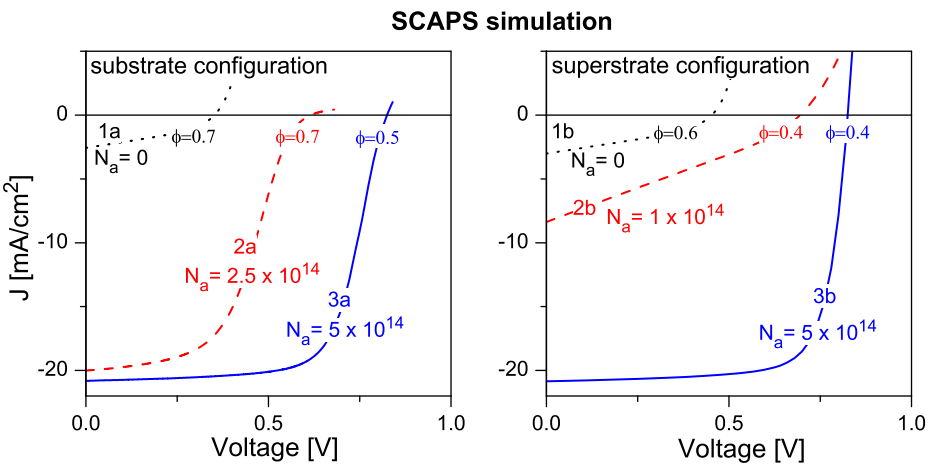

FIG. 7. SCAPS numerical simulations of CdTe solar cell J-V curves varying the two parameters $N_a\,[\mathrm{cm}^{-3}]$ = deep acceptor concentration ($E_a = 220$ meV) and $\varphi\,[\mathrm{eV}]$ = majority carrier barrier height at the back contact. Using these two parameters, the six measured J-V curves shown in Figure 1 can be modeled.

in voltage due to insufficient p-type doping is partially responsible for the low V_{oc}. An additional reduction in V_{oc} is owed to a hole barrier at the back contact.

The low J_{sc} can be attributed to a low collection efficiency. The inset graph in Figure 6 shows the simulated band diagram of a CdTe solar cell with acceptor free absorber. There is only little band bending, which explains the poor carrier separation and the low J_{sc} in Figures 7 and 1.

As an insufficient amount of Cu is added from the front side (substrate configuration Figure 1) some Cu doping (hence band bending) is achieved and the J_{sc} is improved. The Cu amount at the back contact is still too low, hence the barrier height and therefore the V_{oc} limited. This can be modeled by curve 2a in Figure 7.

Cu introduced from the back contact side (superstrate solar cell) on the other hand first leads to a reduced back contact barrier (2b). Only if enough Cu is added, the CdTe becomes sufficiently doped and the J_{sc} increases as a proper p-n junction is established (Figure 7 curve 2b→3b). Note that the measured J-V behavior can be reproduced with a SCAPS model assuming only non-shallow ($E_a = 220$ meV) acceptors.

Figure 8 shows the impact of acceptor concentration and position above the valence band on the CdTe solar cell J-V properties, as calculated by solving the Poisson and continuity equation numerically with SCAPS.[33] The region where today's high efficiency CdTe:Cu solar cells are suspected is marked with a white square. The simulation shows what would happen if one would now change the dopant concentration or introduce acceptor with different position in the bandgap. Note that in all the calculations, the presence of a MGDF of $1 \times 10^{14}\,\mathrm{cm}^{-3}$ was assumed (see Experimental section).

Increasing the dopant concentration generally increases the V_{oc} as expected. However, this is only true as long the respective acceptor level is ionized (compare Figures 5 and 8(a)). As the doping concentration is increased, the SCR size

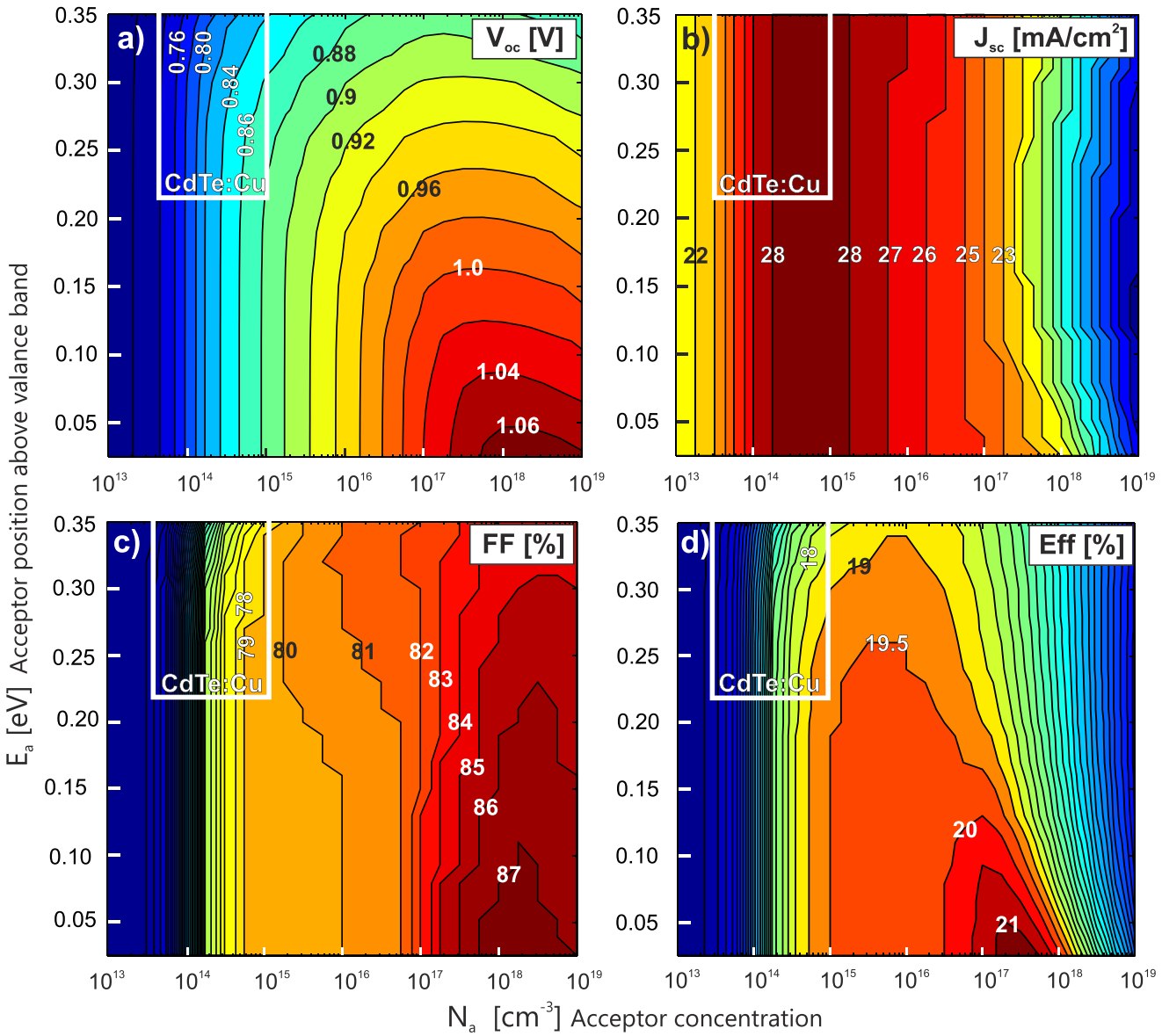

FIG. 8. Calculated solar cell parameters in dependence of acceptor concentration and acceptor position above the valence band in CdTe. The square indicates the region were today high efficiency CdTe:Cu solar cells are suspected.

TABLE I. Simulated solar cell J-V parameters. MGDF denotes the midgap defect concentration, E_a the acceptor position above the valence band and N_a the acceptor concentration.

Cell-label	MGDF [cm^{-3}]	E_a [eV]	N_a [cm^{-3}]	V_{oc} [mV]	J_{sc} [mA/cm^2]	FF [%]	Eff [%]	Remark
TD	1×10^{14}	0.25	4×10^{14}	852	28.0	77.8	18.6	Today's lifetime today's doping
ID	1×10^{14}	0.05	1×10^{17}	1020	24.5	83.1	20.8	Today's lifetime *ideal doping*
IL	0	0.25	4×10^{14}	901	28.3	85.9	21.9	*Ideal lifetime* today's doping
IDL	0	0.05	1×10^{17}	1060	27.0	86.9	25.0	*Ideal doping ideal lifetime*

decreases. The SCR size is the key parameter, which determines the J_{sc}, as electron hole pairs generated outside the SCR heavily recombine. Putting this information together, it is clear that J_{sc} of the solar cell depends on the acceptor concentration as shown in Figure 8(b). The acceptor position hardly influences the J_{sc}. Under the assumptions used in the model discussed here, higher doping will hence always reduce the J_{sc} independent of the acceptor position in the bandgap.

As shown in Figure 8(c), the FF generally increases with higher doping. It should be noted that upon excess Cu introduction, a reduced FF has been observed experimentally.[13,14] This can be understood as we assume that excess Cu introduction does not increase but reduce the net acceptor concentration, which is also indicated by the data shown in Figure 3.

In Figure 8(d), the dependence of conversion efficiency on dopant properties is shown. The counteraction of V_{oc} gain against J_{sc} loss is responsible for a reduced impact of acceptor concentration on the solar cell conversion efficiency in a large doping regime.

Despite the potential for higher V_{oc}, the simulation reveals that even in case the acceptor concentration and depth is optimized, the CdTe solar cell efficiency does not exceed 22%, unless the midgap defect concentration is reduced, and thereby the J_{sc} loss in the high doping regime is avoided.

C. Towards a 25% efficient CdTe solar cell

According to numerical simulations, starting from today's devices, optimizing the doping properties alone will not allow exceeding 22% efficiency.

In Table I, J-V parameters of simulated CdTe solar cells are shown under "today's assumptions" (TD) and with improved properties (ideal doping (ID), ideal liftime (IL) and ideal doping and ideal liftime (IDL)). The simulated solar cell with ID but today deep defect (MGDF) concentration corresponds to the down right corner of Figure 8(d). It reaches 21% efficiency. As the V_{oc} gain is paid by a J_{sc} loss, it is still far away from the theoretical efficiency maximum.[39] The solar cell IL exhibits an ideal lifetime, meaning all deep defects were removed; but with today's doping, the V_{oc} is still below 1 V. Due to the non-ideal J_{sc} and V_{oc}, both solar cells, ID and IL, exhibit less than 22% efficiency. Only as improvements in doping and lifetime are combined (ID + IL = IDL), 25% efficiency is obtained.

It can be concluded that if deep defects are removed and the doping is improved simultaneously, CdTe solar cells can approach the theoretical efficiency limitation close to 30%.[38]

IV. CONCLUSION

The CdTe p-type doping of the CdTe layer in CdTe solar cells can be described with deep acceptors (~300 meV) with low concentration ($N_a = 5 \times 10^{14}\,cm^{-3}$). The Cu induced bulk acceptor concentration in polycrystalline CdTe is 3 orders of magnitude below the overall average Cu concentration in the film. The difference in Cu and acceptor concentration is explained by grain boundary segregation of Cu. According to calculations and experimental data, the Cu induced acceptor Cu_{Cd} is situated at 220–350 meV above the valence band. Calculations show that the Cu_{Cd} bulk acceptors are heavily ionized despite their non-shallow nature.

This understanding was developed based on Hall measurements, solubility and quenching data, and calculation of acceptor ionization (analytically and numerically). Further, the predicted lower formation energy of Cu defects at grain boundaries points into this direction.[8] The commonly observed space charge region size of ~2 μm in CdTe solar cells can also be directly explained by a low acceptor concentration independent of acceptor position in the bandgap.

In order to substantially increase the CdTe solar cell V_{oc}, it is necessary to introduce shallower acceptors in higher concentration. The improvement in device V_{oc} will however be counterbalanced by collection losses of carriers. In order to meet the high theoretical efficiency expectation towards 30%, the CdTe solar cell has to undergo the transformation from a low lifetime drift collection to a high lifetime diffusion collection device.

V. EXPERIMENTAL METHODS

CdTe solar cell growth

CdTe solar cells in superstrate configuration were grown on commercial TEC 15 fluorine doped tin oxide coated SLG. 350 nm CdS (therefore the low J_{sc}) were deposited by high vacuum evaporation followed by 5 μm CdTe. For back contact formation, the CdTe surface was etched with bromine methanol solution after $CdCl_2$ treatment. Subsequently, 0, 0.2, and 3.2 nm Cu were deposited followed by 50 nm of Au and a final annealing in oxygen containing ambient at 215 °C. More details on solar cell processing can be found in literature.[35]

Solar cells in substrate configuration were grown as described by Kranz *et al.*[4] The Cu doping was performed after $CdCl_2$ treatment of CdTe by evaporation of Cu on the CdTe surface and subsequent annealing at 400 °C for 30 min. The sample was cooled down slow (~1 h) if not mentioned different in the text. The Cu amounts added in substrate configuration solar cells shown in Figure 1 were 0, 0.1, and 1.0 angstrom equivalent.

CdTe layer growth and Cu doping

5 μm thick CdTe layers were grown on Corning 7059 BSG glass in high vacuum (1×10^{-6} mbar) at a substrate temperature of 350 °C. 400 nm $CdCl_2$ were deposited and the stack was subsequently annealed at 430 °C in oxygen containing ambient. Cu was deposited in high vacuum and diffusion of Cu into the CdTe layer was promoted by annealing at 400 °C in oxygen containing ambient. Cu thickness was controlled using an Inficon XTM/2 quartz crystal monitor. Line contacts of Au with different distances were deposited by high vacuum evaporation for transmission line method resistivity measurements. Point contacts of Au were deposited to conduct Hall Effect measurements.

Materials purity

Molybdenum oxide MoO_3 from Alfa Aesar with 5N5 purity was used. CdTe from 5N Plus Inc. was used with 6N purity and a Cu concentration <5 ppb (homogenously distributed this would correspond to $<7 \times 10^{13}\,cm^{-3}$ Cu atoms). $CdCl_2$ from Sigma Aldrich with 99.995% purity was used. For CdS growth by chemical bath deposition (CBD) Cadmium acetate hydrate 99.99+% was used with 1 ppm Cu impurity concentration.

Conductivity and contact resistance measurement

Contact resistance and CdTe bulk resistivity were measured using the transmission line method. Au contact distances between 0.2 mm and 2 mm were used. The contact resistance for Cu doped samples was ~5% of the total resistance at 2 mm contact distance.

CV measurement, simulation, and definition of SCR width

Capacitance was measured with an Agilent E4980A precision LCR meter at a frequency of *3*00 kHz. The bias voltage was varied from −1.5 V to 0.5 V. The space charge region width (W_{SCR}) was defined as $W_{SCR} = 1/C^* \varepsilon^* \varepsilon_0$. Also in the simulation, the SCR size was defined as $W_{SCR} = 1/C^* \varepsilon^* \varepsilon_0$, where C is the calculated capacitance by SCAPS.

Hall measurements

Hall measurements were performed using a square geometry with 8 mm side length and Au contacts in the corners. The magnetic field strength was 0.58 T. Measurements were performed at room temperature in dark.

Annealing and quenching

CdTe layers or solar cells were annealed for 10 min at 210 °C in air. Subsequently, the layers were quenched by dipping into ice water.

Solar cell characterization

Current density–voltage (J–V) measurements were performed under standard testing conditions (AM1.5 G, 1000 W/cm^2, and cell temperature 25 °C). External quantum efficiency (EQE) was measured under white bias light (halogen lamp). J_{sc} values were calculated using the reference spectrum IEC 60904-3 Ed.2.

SIMS measurement of Cu in CdTe/CdS solar cells

Cu distribution in the solar cell was measured with TOF-SIMS. The instrument was built by ION-TOF. Bi_1^+ ions with 25 keV energy, and a current of 1 pA were used. An area of $(100\,\mu m)^2$ was analyzed and positive secondary ions were detected. Sputtering of an area of $(300\,\mu m)^2$ was performed using O_2^+ at an energy of 2 kV and a current of 400 nA.

Numerical and analytical calculations, general settings

All simulations were performed with SCAPS version 3.2.01. The CdTe base definition (22.05.2009) provided with this SCAPS version was used. For all calculations (if not mentioned different), the hole capture cross section of the MGDF was increased from $1 \times 10^{-15}\,cm^{-2}$ to $1 \times 10^{-13}\,cm^{-2}$ (following Ref. 36). The shallow acceptor concentration was set to zero for all calculations.

Calculation of acceptor ionization degree (Figure 5)

The CdTe thickness was set to 10 μm in order to eliminate the junction influence. A single acceptor was introduced and concentration and depth were varied as shown in Figure 5. The ionization degree was defined as minimum acceptor defect occupation (around the center of the CdTe). Calculation with formula 2 were performed using the same parameters as defined in the SCAPS calculation ($N_V = 1.8 \times 10^{19}\,cm^{-3}$).

Simulation of SCR width

The CdTe base definition file was modified as described under general settings above. A single acceptor defect 350 meV above the valance band with $1 \times 10^{17}\,cm^{-3}$ concentration was introduced. A shallow single donor 25 meV below the conduction band with $1 \times 10^{16}\,cm^{-3}$ concentrations was added. The capacitance calculated was 41 nF/cm^2 and the SCR according to $W_{SCR} = 1/C^* \varepsilon^* \varepsilon_0 = 202$ nm.

Simulation of QE with and without midgap defect (Figure 6)

The red dashed line was calculated under illumination without further changes in settings. The blue dashed-dotted line is achieved as the MGDF concentration is set to zero or the hole capture cross section is $<\sim 1 \times 10^{-15}\,cm^{-2}$. The energy band diagram was calculated under illumination at 0 V (short circuit condition).

Simulation of CdTe solar cell J-V (Figure 7)

Back contact barrier and deep acceptor (220 meV) concentration is assumed as given in the figure. No further changes to the settings were performed. To also correctly simulate the J_{sc}, one would need to account for the different transparent conducting oxide and CdS thickness used. For

simplicity, the simulation was restricted to the basic phenomena.

Simulation of Voc, Eff, Jsc, FF versus acceptor properties (Figure 8)

In order to simulate an enhanced champion CdTe material quality compared to our baseline CdTe, the MGDF concentration was reduced by 50% to $1 \times 10^{14}\,cm^{-3}$.

A deep single acceptor level was introduced 220 meV above E_V (following Wei *et al.*[6]) and $3 \times 10^{14}\,cm^{-3}$ concentration. CdS thickness was reduced to 0.002 μm and the optical filter at the font contact was removed. These settings represent state of the art devices ($V_{oc} = 846\,mV$, $J_{sc} = 28.0\,mA/cm^2$, FF = 76.9%, and Eff = 18.2%). Starting from this point, the acceptor defect concentration and position is varied from $1 \times 10^{13}\,cm^{-3}$ to $1 \times 10^{18}\,cm^{-3}$ and 0.025 to 0.35 eV, respectively.

Simulation of solar cell examples (Table I)

Apart from the values given in Table I, all parameters were identical with the calculation of Figure 8.

ACKNOWLEDGMENTS

We gratefully acknowledge partial funding from Swiss National Science foundation under the Contract No. 200021_127035. Financial supports from National Science Foundation (SNF), (Contract no. 200021_127035) and from the Competence Center Energy and Mobility in ETH-Domain (CCEM-Dursol) are gratefully acknowledged.

[1]E. I. Adirovich, Y. M. Yuabov, and G. R. Yagudaev, *Photoelectric Effect in Film Diodes with CdS-CdTe Heterojunctions* (Physicotechnical Institute, Academy of Sciences of the Uzbek SSR, 1969).
[2]X. Wu, Sol. Energy **77**(6), 803–814 (2004).
[3]J. V. Li, J. N. Duenow, D. Kuciauskas, A. Kanevce, R. G. Dhere, M. R. Young, and D. H. Levi, in *IEEE Photovoltaic Specialists Conference* (Austin, Texas, 2012).
[4]L. Kranz, C. Gretener, J. Perrenoud, R. Schmitt, F. Pianezzi, F. L. Mattina, P. Blösch, E. Cheah, A. Chirilă, C. M. Fella, H. Hagendorfer, T. Jaeger, S. Nishiwaki, A. R. Uhl, S. Buecheler, and A. N. Tiwari, "Doping of polycrystalline CdTe for high-efficiency solar cells on flexible metal foil," Nat. Commun. **4**, 2306 (2013).
[5]B. Biglari, M. Samimi, M. Hage-Ali, J. M. Koebel, and P. Siffert, J. Cryst. Growth **89**(4), 428–434 (1988).
[6]S.-H. Wei and S. B. Zhang, Phys. Rev. B **66**(15), 155211 (2002).
[7]D. Krasikov, A. Knizhnik, B. Potapkin, S. Selezneva, and T. Sommerer, Thin Solid Films **535**, 322–325 (2013).
[8]L. Zhang, J. L. F. Da Silva, J. Li, Y. Yan, T. A. Gessert, and S.-H. Wei, Phys. Rev. Lett. **101**(15), 155501 (2008).
[9]J. Ma, S.-H. Wei, T. A. Gessert, and K. K. Chin, Phys. Rev. B **83**(24), 245207 (2011).
[10]V. I. Kaydanov and T. R. Ohno, "Studies of basic electronic properties of CdTe-based solar cells and their evolution during processing and stress," Report No. NREL/SR-520-41129 (2007).
[11]K. K. Chin, Sol. Energy Mater. Sol. Cells **94**(10), 1627–1629 (2010).
[12]A. D. Compaan, A. Gupta, S. Lee, S. Wang, and J. Drayton, Sol. Energy **77**(6), 815–822 (2004).
[13]S. Demtsu, D. Albin, and J. Sites, paper presented at the IEEE 4th World Conference on Photovoltaic Energy Conversion (WCPEC-4), Waikoloa, Hawaii, 2006.
[14]T. A. Gessert, S. Asher, S. Johnston, A. Duda, M. R. Young, and T. Moriarty, paper presented at the Conference Record of the IEEE 4th World Conference on Photovoltaic Energy Conversion, Waikoloa, Hawaii, 2006.
[15]E. Kučys, J. Jerhot, K. Bertulis, and V. Bariss, Phys. Status Solidi A **59**(1), 91–99 (1980).
[16]K. K. Chin, T. A. Gessert, and W. Su-Huai, paper presented at the 35th IEEE Photovoltaic Specialists Conference (PVSC), Honolulu, Hawaii, 2010.
[17]G. Teeter and S. Asher, *Modeling Cu Migration in CdTe Solar Cells Under Device-Processing and Long-Term Stability Conditions,* paper presented at the IEEE 33th Photovoltaic Specialist Conference, San Diego, California, 2008.
[18]Y. Yan, K. Jonesa, J. Zhoua, X. Wua, and M. Al-Jassima, Mater. Res. Soc. Symp. Proc. **1012**, Y04-09 (2007).
[19]H. H. Woodbury and M. Aven, J. Appl. Phys. **39**(12), 5485–5488 (1968).
[20]V. I. Grytsiv, Ph.D. Thesis, Cernovey, 1975.
[21]E. D. Jones, N. M. Stewart, and J. B. Mullin, J. Cryst. Growth **117**(1–4), 244–248 (1992).
[22]U. V. Desnica and N. B. Urli, Phys. Rev. B **6**(8), 3044–3053 (1972).
[23]V. Consonni, G. Feuillet, J. P. Barnes, and F. Donatini, Phys. Rev. B **80**(16), 165207 (2009).
[24]M. H. Du, Phys. Rev. B **80**(20), 205322 (2009).
[25]S. A. Awadalla, A. W. Hunt, K. G. Lynn, H. Glass, C. Szeles, and S.-H. Wei, Phys. Rev. B **69**(7), 075210 (2004).
[26]A. Balcioglu, R. K. Ahrenkiel, and F. Hasoon, J. Appl. Phys. **88**(12), 7175–7178 (2000).
[27]A. A. Gippius, J. R. Panossian, and V. A. Chapnin, Phys. Status Solidi A **21**(2), 753–758 (1974).
[28]F. A. Kröger, Rev. Phys. Appl. (Paris) **12**(2), 205–210 (1977).
[29]A. S. Gilmore, V. Kaydanov, and T. R. Ohno, Mater. Res. Soc. **763**, B9.6.1–B9.6.6 (2003).
[30]J. P. Chamonal, E. Molva, and J. L. Pautrat, Solid State Commun. **43**(11), 801–805 (1982).
[31]M. Said and M. A. Kanehisa, J. Cryst. Growth **101**(1–4), 488–492 (1990).
[32]J. S. Blakemore, *Semiconductor Statistics* (Pergamon Press, 1962).
[33]R. Scaburri, "The incomplete ionization of substitutonal dopants in silicon carbide," Doctoral Tesis, Universita di Bologna (2011).
[34]M. Burgelman, P. Nollet, and S. Degrave, Thin Solid Films **361–362**, 527–532 (2000).
[35]M. H. Du, H. Takenaka, and D. J. Singh, J. Appl. Phys. **104**(9), 093521–093529 (2008).
[36]J. Perrenoud, L. Kranz, S. Buecheler, F. Pianezzi, and A. N. Tiwari, Thin Solid Films **519**(21), 7444–7448 (2011).
[37]R. Scheer and H. W. Schock, *Chalcogenide Photovoltaics* (Wiley-VCH, 2011).
[38]A. O. Pudov, M. Gloeckler, S. H. Demtsu, J. R. Sites, K. L. Barth, R. A. Enzenroth, and W. S. Sampath, paper presented at the Conference Record of the 29th IEEE Photovoltaic Specialists Conference, New Orleans Louisiana, 2002.
[39]W. Shockley and H. J. Queisser, "Detailed balance limit of efficiency of p-n junction solar cells," J. Appl. Phys. **32**(3), 510–519 (1961).